

Structural Investigation of the Binding of a Herpesviral Protein to the SH3 Domain of Tyrosine Kinase Lck^{†,‡}

Kristian Schweimer,[§] Silke Hoffmann,[§] Finn Bauer,[§] Ute Friedrich,^{||} Christian Kardinal,[⊥] Stephan M. Feller,[#] Brigitte Biesinger,^{||,△} and Heinrich Sticht^{*,§}

Lehrstuhl für Biopolymere, Universität Bayreuth, 95440 Bayreuth, Germany, Institut für Klinische und Molekulare Virologie, Universität Erlangen-Nürnberg, 91054 Erlangen, Germany, Medizinische Hochschule Hannover, 30623 Hannover, Germany, Cell Signalling Laboratory, Imperial Cancer Research Fund, University of Oxford, Oxford OX3 9DS, U.K., and Max-Planck-Institut für Biochemie, Am Klopferspitz 18A, 82152 Martinsried, Germany

Received November 28, 2001; Revised Manuscript Received February 11, 2002

ABSTRACT: Herpesvirus saimiri codes for a tyrosine kinase interacting protein (Tip) that interacts with both the SH3 domain and the kinase domain of the T-cell-specific tyrosine kinase Lck via two separate motifs. The activation of Lck by Tip is considered as a key event in the transformation of human T-lymphocytes during herpesviral infection. We investigated the interaction of proline-rich Tip peptides with the LckSH3 domain starting with the structural characterization of the unbound interaction partners. The solution structure of the LckSH3 was determined by heteronuclear multidimensional nuclear magnetic resonance (NMR) spectroscopy using 44 residual dipolar couplings in addition to the conventional experimental restraints. Circular dichroism spectroscopy proved that the polyproline helix of Tip is already formed prior to SH3 binding and is conformationally stable. NMR titration experiments point out three major regions of the Tip–Lck interaction comprising the RT loop, the n-src loop, and a helical turn preceding the last strand of the β -sheet. Further changes of the chemical shifts were observed for the N- and C-terminal β -strands of the SH3 domain, indicating additional contacts outside the proline-rich segment or subtle structural rearrangements transmitted from the binding site of the proline helix. Fluorescence spectroscopy shows that Tip binds to the SH3 domains of several Src kinases (Lck, Hck, Lyn, Src, Fyn, Yes), exhibiting the highest affinities for Lyn, Hck, and Lck.

Protein tyrosine kinases are critically involved in signaling pathways that regulate cell growth, differentiation, activation, and transformation. Nonreceptor tyrosine kinases belonging to the Src family are key players in signal transduction, and much effort has been made in order to understand their physiological role as well as their regulation. Some Src kinases (Fyn, Src, Yes) are found in most cell types whereas others exhibit a more restricted tissue distribution (Lck, Hck, Blk) and have more specific tasks in signal transduction. Lck is a lymphoid-specific member of this family that is essential for T-cell development and function. It is tightly associated with the cytoplasmic parts of the CD4 and CD8 receptors and catalyzes the initial phosphorylation of T-cell receptor components necessary for signal transduction and T-cell activation (1–3). Lck exhibits a molecular architecture

typical for the Src family of tyrosine kinases (Src, Blk, Fgr, Fyn, Hck, Lck, Lyn, Yes, Yrk): a myristylated N-terminal “unique” domain is followed by the regulatory SH3¹ and SH2 domains and by the kinase domain containing the active site. The C-terminal region contains a regulatory tyrosine residue (Tyr505) which is bound to the SH2 domain in its phosphorylated form, thereby reducing kinase activity. Further understanding of the regulation of Lck has been provided by the crystal structures of c-Src (4, 5) and Hck (6). From these structures it can be inferred that also the SH3 and SH2 domains function in part to negatively regulate kinase activity by forming intramolecular contacts that stabilize the catalytic domain in an inactive conformation. Release of these intramolecular regulatory constraints by dephosphorylation of Tyr505 (7) or by the presence of SH2/SH3 competing ligands (8) results in the autophosphorylation of Tyr394 in the activation loop and a catalytically active kinase (9).

Tyrosine kinases, however, do not only play a role in “normal” intracellular processes but are frequently targeted

[†] This work was supported by grants from the Deutsche Forschungsgemeinschaft (DFG) to H.S. (SFB 466, A6) and B.B. (SFB 466, B2) and by the Fonds der Chemischen Industrie to H.S.

[‡] The coordinates have been deposited in the Brookhaven Protein Data Bank (file name 1H92).

^{*} To whom correspondence should be addressed. Tel: +49 921 553542. Fax: +49 921 553544. E-mail: Heinrich.Sticht@Uni-Bayreuth.de.

[§] Universität Bayreuth.

^{||} Universität Erlangen-Nürnberg.

[⊥] Medizinische Hochschule Hannover.

[#] University of Oxford.

[△] Max-Planck-Institut für Biochemie.

¹ Abbreviations: CD, circular dichroism; COSY, correlated spectroscopy; HSQC, heteronuclear single-quantum coherence; HVS, Herpesvirus saimiri; NMR, nuclear magnetic resonance; NOE, nuclear Overhauser effect; RDC, residual dipolar coupling; RMSD, root mean square deviation; SH3, Src-homology domain 3; TFE, trifluoroethanol; Tip, tyrosine kinase interacting protein; TOCSY, total correlation spectroscopy.

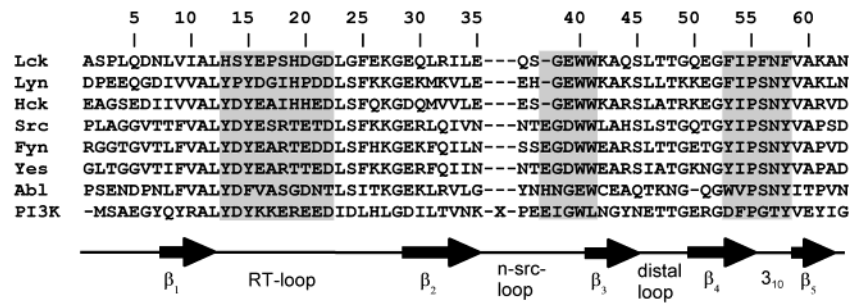


FIGURE 1: Sequence alignment of the SH3 domains from the tyrosine kinases Lck, Lyn, Hck, Src, Fyn, Yes, and Abl and from phosphatidylinositol 3-kinase (PI3K). The numbering scheme of the LckSH3 domain used in the present study is given at the top. The X marks a 15-residue insertion in the PI3K sequence that is not present in the other SH3 domains shown in the alignment. Elements of secondary structure found in the structure of LckSH3 are given below the alignment. Gray boxes highlight those stretches of amino acids that are known to interact with proline-rich ligands.

by viral effector molecules to ensure their own replication and/or persistence. Consequently, Lck is targeted by regulatory proteins of T-lymphotrophic viruses, for example, by Herpesvirus saimiri (HVS) tyrosine kinase interacting protein (Tip). HVS is able to induce leukemia and lymphoma in New World primates and to immortalize monkey lymphocytes (10). In addition, HVS strain C488 is able to transform human T-cells to permanent growth in vitro (11). Two viral gene products, StpC and Tip, are required for the T-cell transforming phenotype of HVS C488 (12). The T-cell specificity is attributed to Tip, which has been identified as a binding partner and in vitro substrate of Lck (13) and causes lymphoma when inducibly expressed in transgenic mice (14).

Tip proteins from HVS subgroup C strains contain a stretch of 38 amino acids which is both necessary and sufficient for Lck binding (15, 16). This binding region contains a segment that shows a significant sequence similarity to the carboxy-terminal region of several kinases of the Src family and a proline-rich segment. These two sequence motifs that are separated by approximately 20 amino acids were shown to bind to the kinase domain and the SH3 domain of Lck, respectively (16, 17). Expression of Tip in Jurkat T-cells reduces the activation-induced tyrosine phosphorylation of cellular proteins (18), indicating a functional inhibition of Lck in vivo. However, in several cell-free assay systems, interaction with Tip induces the phosphotransferase activity of Lck (19–22), and both motifs involved in Lck binding are required for activation of the kinase (16).

Structural studies of the interaction between Tip and Lck are therefore expected to contribute to the understanding of the mechanisms of T-cell growth regulation and of herpesviral pathogenicity. In addition, understanding the regulation of Lck activity by Tip may serve as a basis for the development of new drugs capable of modifying Lck activity in different pathological situations (23). The size of the Tip–Lck complex of >60 kDa, however, hampers a structural investigation of the system by NMR spectroscopy. Therefore, our approach is based on the dissection of Src family tyrosine kinases into their individual domains that have suitable sizes for NMR spectroscopic studies. Here, we describe the interaction of Tip fragments containing the proline-rich SH3 binding motif with the SH3 domains of Lck and related tyrosine kinases. To allow a more detailed understanding of the Tip–Lck interaction, both components were first structurally characterized in the unbound form and then in the binary complex.

MATERIALS AND METHODS

Cloning, Expression, and Purification of LckSH3 for NMR Spectroscopic Studies. Nucleotides comprising the SH3 domain of Lck (aa 59–119, LckSH3) were cloned via PCR from the expression system pGEX-NT+SH3 (17) into the *Bam*HI and *Eco*RI restriction sites of pGEX-4T-2 using the oligonucleotide SH3_5' (gga gga gga tcc cca ctg caa gac aac ctg g) and a commercially available pGEX reverse sequencing primer (Pharmacia). The resulting vector pGEX-4T-LckSH3 provides an NH₂-terminal glutathione *S*-transferase (GST) affinity tag cleavable with thrombin protease. Thrombin cleavage of the GST–LckSH3 fusion protein ends in an LckSH3 peptide with an additional Gly and a Ser residue at its NH₂ terminus. Therefore, the 63 aa LckSH3 peptide used in this study corresponds to aa 57–119 of the original Lck with an A57G mutation. The numbering scheme used throughout this paper will refer to the expressed protein, starting from the mutated Gly1 instead of Gly57 (Figure 1).

For overexpression of the GST–LckSH3 fusion protein *Escherichia coli* strain BL21 was transformed with pGEX-4T-LckSH3. Cells were induced with 1 mM IPTG and harvested after 3 h of growth at 37 °C. For ¹⁵N labeling M9 minimal medium was used with [¹⁵N]ammonium chloride as the sole nitrogen source. LckSH3 was purified using affinity chromatography on glutathione–Sepharose (GSTrap, Pharmacia) using an ÄKTA system (Pharmacia). Fractions containing pure GST–LckSH3 fusion protein were dialyzed against cleavage buffer (20 mM Tris-HCl, pH 8.4, 150 mM NaCl, 2.5 mM CaCl₂, 2.5 mM BME), and thrombin cleavage was performed using 0.5 unit of thrombin protease (Novagen) per 1 mg of fusion protein for 6 h at room temperature. Protease cleavage was stopped by addition of PMSF to a final concentration of 0.5 mM. The LckSH3 peptide was separated from the uncleaved fusion protein, GST, and thrombin using a Superdex 75 preparative grade gel filtration column on an ÄKTA system (Pharmacia), which was equilibrated with cleavage buffer. LckSH3 peptide-containing fractions were checked by SDS–PAGE, dialyzed against 2 mM potassium phosphate, pH 6.4, with 1 mM NaCl, and concentrated by lyophilization.

Peptide Synthesis. The chemically synthesized peptides ATWDPGMPTPLPPRPANLG and GMPTPLPPRPAN comprising residues 168–187 and 173–185 of Tip, respectively, as well as a mutant Tip protein in which W170 is replaced by leucine were either synthesized in house (C. Kardinal, unpublished) or purchased from Biosyntan (Berlin).

CD Spectroscopy. Far-UV CD spectra of Tip(168–187), Tip(168–187) W170L, and Tip(173–185) were recorded at 298 K in H₂O, pH 6.3, in a 0.1 cm cell from 180 to 260 nm at 20 nm/min on a Jasco J 810 CD spectropolarimeter at a peptide concentration of 50 μ M. The reference sample contained pure water. Spectra were measured 10 times and averaged for each peptide and the reference sample. The ellipticity Θ was calculated in millidegrees instead of the $[\Theta]_{MRW}$ value in order to allow a comparison of the overall content of secondary structure in peptides of different length (24).

Titration experiments were performed by addition of increasing amounts of trifluoroethanol (TFE) to a 5 μ M Tip-(168–187) sample in a 1 cm cell, collecting spectra from 190 to 260 nm. The sample was stirred for proper mixing, and the change of Tip concentration as a result of TFE addition was corrected.

Fluorescence Spectroscopy and Calculation of the Binding Constant. Measurements were performed essentially as previously described (25) in a Perkin-Elmer 760–40 fluorescence spectrophotometer at an excitation wavelength of 290 nm (slit width, 2 nm) and an emission wavelength of 345 nm (slit width, 17 nm). A mini magnetic stirrer was used to mix the solution in a 1 cm² quartz fluorescence cell. A circulating water bath was used to maintain the sample temperature at 291 K. To obtain the titration curves for calculation of the binding constants, peptides from a stock solution of 5 mg/mL in PBS–1 mM dithiothreitol were added in small increments to 3 mL of PBS–1 mM dithiothreitol containing 50 μ g of GST–SH3 domain fusion proteins. Upon addition of the peptide solution, changes in fluorescence were measured. Since the concentration of the SH3 domain-containing protein was low (\sim 0.5 μ M), the experimental data were fitted to the equation $F = F_{max} \cdot [\text{peptide}] / (K_d + [\text{peptide}])$, where [peptide] is the final peptide concentration at each measurement point, F is the measured protein fluorescence intensity at the particular peptide concentration, and F_{max} is the observed maximal fluorescence intensity of the protein when saturated with the peptide. Nonlinear regression curve fitting was carried out to fit the experimental data to the equation, with F_{max} and K_d as fitted parameters. The change in protein concentration that occurred as a result of peptide addition was properly corrected.

NMR Spectroscopy. All NMR experiments were performed on a Bruker DRX 600 MHz spectrometer with pulsed field gradient capabilities at a temperature of 298 K. NMR samples for the structure determination of the free LckSH3 domain contained 1.5 mM ¹⁵N-labeled or ¹⁵N/¹³C-labeled protein in 50 mM potassium phosphate and 20 mM sodium chloride, pH 6.4, in H₂O/D₂O (9:1). For assignment of the backbone and H β /C β chemical shifts the following set of experiments were recorded: 2D ¹H, ¹⁵N FHSQC (26), 3D CT-HNCO, 3D CT-HNCA (27), 3D HNCACB (28), 3D CBCA(CO)-NH (29), 3D HNHA (30, 31), and 3D HBHA(CO)NH (32). For further aliphatic ¹³C/¹H assignments 3D C(CO)NH and 3D H(CCO)NH (33), ¹H–¹³C CT-HSQC (34), and 3D H(C)-CH-COSY with gradient coherence selection (35) were recorded. A ¹⁵N NOESY HSQC and a ¹³C NOESY HSQC were recorded with a mixing time of 120 ms for deriving distance restraints for structure calculation. Aromatic proton resonances were assigned from ω_2 ¹⁵N-filtered NOESY and

TOCSY experiments (36) with mixing times of 120 and 80 ms, respectively.

Slowly exchanging amide protons were identified from a series of ¹⁵N/¹H HSQCs that were recorded 23, 45, 67, 89, 111, 133, 155, 177, 199, 221, and 243 min after lyophilized protein was dissolved in D₂O. The {¹H}¹⁵N NOE experiments were recorded using the pulse sequences of Dayie and Wagner (37). The relaxation delay was 4 s, and the proton saturation was performed by 120° high-power pulses with an interpulse delay of 5 ms for the final 3 s of the relaxation delay of the saturation experiment.

For measuring residual dipolar couplings a solution of ¹⁵N-labeled LckSH3 (0.5 mM) in the DHPC–DMPC bicelle system (molar ratio 1:3, 3% w/v bicelles) was used at a temperature of 302 K. The isotropic scalar couplings were measured at the same temperature using a sample without bicelles. The IPAP methodology (38, 39) was applied for recording the NH splittings. The dipolar couplings were calculated from the difference of the NH splitting in the oriented phase and the isotropic phase. For each sample at least three repetitions of a IPAP experiment were conducted to estimate the error of the measured coupling values.

The binding of Tip to LckSH3 was followed by chemical shift disturbance measured by ¹H, ¹⁵N HSQC experiments during titration of Tip to the ¹⁵N-labeled SH3 domain. Using starting concentrations of 0.8 mM for LckSH3 and a 5 mM stock solution of Tip(173–185) or Tip(168–187), the titrations were performed to an at least 4-fold excess of Tip. For the assignment of the side-chain resonances and the identification of distance restraints 3D CBCA(CO)NH and H(C)CH-COSY as well as a ¹⁵N and a ¹³C NOESY HSQC experiment with 120 ms mixing time were measured for Tip-bound LckSH3. D₂O exchange and {¹H}¹⁵N NOE experiments were recorded in an identical fashion as described above for the unbound LckSH3 domain. The NMR data sets were processed using in-house written software and analyzed with the program packages NMRView (40) and NDEE (SpinUp Inc., Dortmund, Germany).

Structure Calculation and Analysis. On the basis of the almost complete assignment of the ¹H, ¹³C, and ¹⁵N resonances of the unbound LckSH3 domain, a total of 346 NOE distance restraints (including 213 long-range NOEs) could be derived from the two- and three-dimensional NOESY spectra in an iterative procedure (Table 1). NOE cross-peaks were manually classified as strong, medium, or weak according to their intensities and converted into distance restraints of less than 2.7, 3.5, or 5.0 Å, respectively. A total of 31 residues showed ³J_{HNH α} scalar coupling constants of either <6.0 Hz or >8.0 Hz and were therefore restrained to adopt backbone torsion angles between –80° and –40° or between –160° and –80°, respectively. A hydrogen bond was assumed if the acceptor of a slowly exchanging amide proton could be identified unambiguously from the results of initial structure calculations. For each of the 14 hydrogen bonds the distance between the amide proton and the acceptor was restrained to less than 2.3 Å and the distance between the amide nitrogen and the acceptor to less than 3.1 Å. These experimental restraints served as an input for the calculation of 120 structures using restrained molecular dynamics with X-PLOR 3.851 (41). To this end a three-stage simulated annealing protocol (42) with floating assignment of prochiral groups (43) was carried out using the

Table 1: Summary of Structure Calculation

Experimental Restraints for Final Structure Calculation		
interresidual NOEs		341
sequential ($ i - j = 1$)		77
medium range ($ i - j \leq 5$)		51
long range ($ i - j > 5$)		213
intraresidual NOEs		5
dihedral angle restraints		
$^3J(\text{H}^N, \text{H}^\alpha)$		31
hydrogen bonds		24
restraints from dipolar couplings		44
Molecular Dynamics Statistics ^a		
average energy (kcal/mol)		
E_{tot}		66.32 (± 0.67)
E_{bond}		1.02 (± 0.05)
E_{angles}		54.95 (± 0.37)
E_{improper}		6.81 (± 0.14)
E_{repel}		0.80 (± 0.16)
E_{NOE}		1.16 (± 0.19)
E_{cdih}		0.03 (± 0.03)
E_{dipo}		1.54 (± 0.04)
RMSD from ideal distances (\AA)		
NOE		0.018 (± 0.0003)
bonds		0.001 (± 0.000025)
RMSD from ideal angles (deg)		
bond angles		0.453 (± 0.002)
improper angles		0.321 (± 0.002)
RMSD from dipolar couplings (Hz)		
H-N couplings		0.021 (± 0.182)
Atomic RMS Differences (\AA)		
	backbone	heavy atoms
SH3 fold ^b	0.37	0.84
regular secondary structure ^c	0.28	0.84
SA _{RDC} vs SA _{noRDC} ^d	0.73	0.92
SA _{RDC} vs ILCK ^d	0.96	1.34
SA _{noRDC} vs ILCK ^d	1.00	1.41

^a The final force constants used in the structure calculations were 1000 kcal·mol⁻¹·Å⁻² for the bond length, 500 kcal·mol⁻¹·rad⁻² for the bond angles and improper angles, 50 kcal·mol⁻¹·Å⁻² for the NOE distance restraints, 5.0 kcal·mol⁻¹·rad⁻² for the φ -angle restraints, and 1.0 kcal·mol⁻¹·Hz⁻² for the residual dipolar couplings. ^b Calculated for the final set of 30 structures (residues 7–61). ^c Calculated for the final set of 30 structures (residues 8–11, 29–35, 41–45, 50–55, and 59–61). ^d SA_{RDC}, average structure of the final 30 structures calculated with dipolar couplings; SA_{noRDC}, average structure of 30 structures from a control simulation calculated without dipolar couplings; ILCK, crystal structure of the LckSH3 (55). All comparisons were performed for residues 7–61.

following simulation procedure: For conformational space sampling 60 ps with a time step of 2 fs was simulated at a temperature of 2000 K, followed by 80 ps of slow cooling to 1000 K, and 60 ps of cooling to 100 K, both with a time step of 1 fs. A conformational database term for both backbone and side-chain dihedral angles (44) with the modification described in Neudecker et al. (45) was included in the target function in order to improve the stereochemical properties of the structures. After simulated annealing the structures were subjected to 1200 steps of energy minimization, the final 1000 steps without conformational database potential.

The axial component and rhombicity of the alignment tensor were obtained by a grid search procedure using the tensor components of the structures calculated without RDCs as starting values. The initial values of the alignment tensor were calculated in a least-squares manner on the basis of the measured coupling values and the structures obtained with NOEs, hydrogen bonds, and J -couplings as described

by Losonczi et al. (46) using in-house written MATLAB scripts. The width of the grid was 0.5 Hz for the axial component and 0.05 for the rhombicity, respectively, and for each point of the grid a set of 60 structures was calculated. The X-PLOR potential energy term for the dipolar couplings was included in the target function of the simulated annealing protocol during the cooling stages, gradually increasing the force constant from 0.01 to 1.0 kcal mol⁻¹ Hz⁻². For each set of structures, RDCs were calculated and compared to the experimentally measured values. The value of the alignment tensor resulting in the best agreement between measured and calculated RDCs was used for the final calculation.

Of the 120 structures resulting from the final round of structure calculation, the 30 lowest energy structures having no NOE distance restraint violations greater than 0.1 Å and no φ -angle restraint violations greater than 0.5° were selected for further characterization. The geometry of the structures, structural parameters, and elements of secondary structure were analyzed using the programs DSSP (47), MOLMOL (48), PROCHECK (49), and PROMOTIF (50). For the graphical presentation of the structures SYBYL 6.5 (Tripos Associates), MOLSCRIPT (51), and Raster3D (52) were used.

RESULTS AND DISCUSSION

Assignment and Structure of the LckSH3 Domain. Most of the ¹H^N, ¹⁵N, ¹³C^α and ¹³C^β resonances could be automatically assigned sequentially using an in-house written search algorithm based on inter- and intraresidual C^α and C^β chemical shifts taken from the CBCA(CO)NH and HNCACB spectra for sequential linking of amide resonances and amino acid type determination. No unambiguous assignment could be made for the two N-terminal residues due to the lack of sequential connectivities, suggesting that these residues are unstructured in solution. For aliphatic side chains complete carbon and proton assignments were made from the 3D H(C)CH-COSY, C(CO)NH, and HC(CO)NH spectra, while aromatic proton resonances were assigned from homonuclear 2D spectra and from the ¹³C-edited 3D NOESY. On the basis of these types of experiments, all proton side-chain resonances of residues 3–63 could be assigned with exception of four aromatic resonances (H^ε, H^δ) for which a strong signal overlap was present in the spectra.

The calculation of the final structures was based on 346 interresidual distance restraints, 31 φ angle restraints, 26 hydrogen bond restraints, and 44 restraints from RDCs (Table 1). According to PROCHECK (49) analysis of the family of 30 structures all residues show energetically favorable backbone conformations: 91% of the residues are found in the most favored regions and 9% in the allowed regions of the Ramachandran plot.

Subsequent analysis was restricted to the rigid SH3 “core fold” (residues 7–61) that is generally characterized by heteronuclear NOE values larger than 0.5 (Figure 3A). The structure of residues 7–61 is well-defined (Figure 2A), showing average root mean square deviations (RMSDs) of 0.37 and 0.84 Å for the backbone heavy atoms and all heavy atoms, respectively (Table 1).

Inclusion of the RDCs did not significantly change the precision of the calculated structures as estimated from a

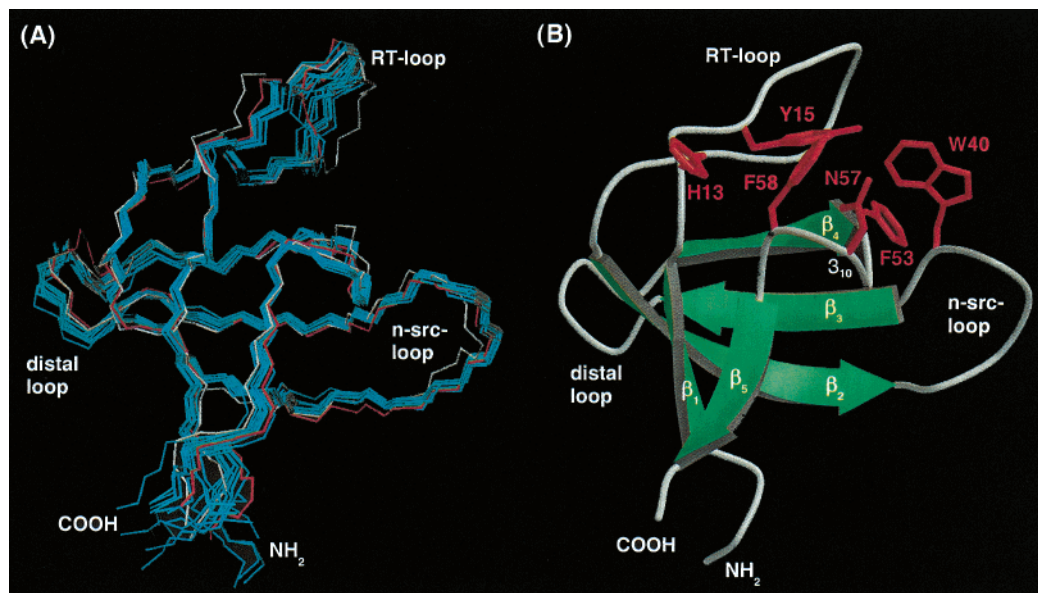


FIGURE 2: (A) Overlay of a set of 10 LckSH3 structures (residues 7–61) that was calculated using 44 additional restraints from residual dipolar couplings (cyan). For comparison the LckSH3 crystal structure (PDB code 1LCK) and the average structure of a family of structures calculated without dipolar couplings are shown in white and red, respectively. For clarity, the flexible residues are omitted in the figure. (B) Schematic presentation of the LckSH3 structure (residues 5–63) indicating the elements of secondary structure. The conserved residues that are known to be important for ligand binding are shown as red sticks, and the loops are labeled. Figure prepared with Sybyl 6.5 (Tripos Associates), Molscript (51), and Raster3D (52).

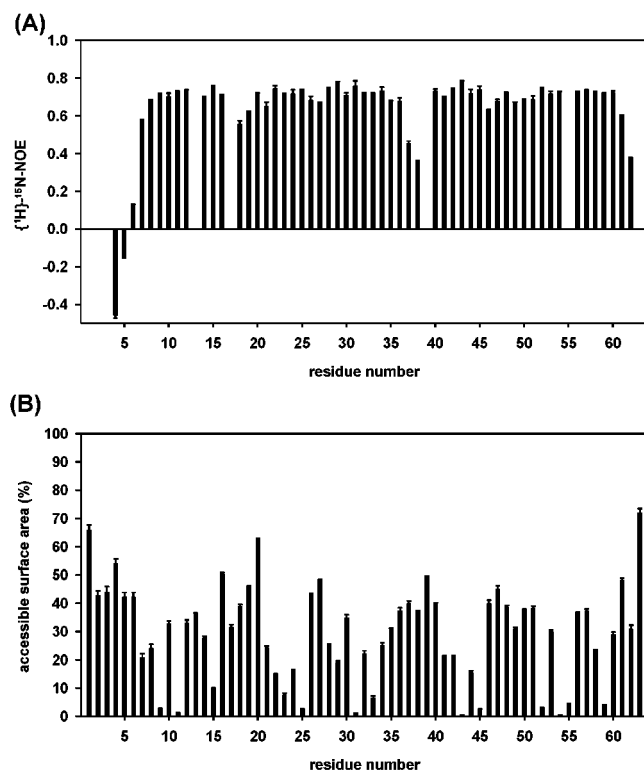


FIGURE 3: (A) Magnitude of the $\{^1\text{H}\}^{15}\text{N}$ heteronuclear NOE (I_{sat}/I_0) along the amino acid sequence. (B) Solvent-accessible surface area per residue. Values were calculated with MOLMOL (48) and represent average values over the set of 30 final structures. Error bars are shown on the top of each bar.

control simulation without RDCs, resulting in a backbone RMSD of 0.38 Å. The RMSD between the average structures from both calculations is 0.73 Å, showing that the restraints derived for the orientation of the H–N vectors confirm the overall backbone topology established on the basis of the conventional NMR data.

Analysis of the structure reveals five antiparallel β -strands (L8–A11, L29–E35, W41–S45, Q50–P55, and V59–K61) forming two triple-stranded β -sheets packed at almost right angles (Figures 1 and 2). One prominent feature is a twist in the central strand β_2 that allows it to participate in both β -sheets. The first sheet is formed by β -strands β_1 , β_5 , and the first half of β_2 , while the second β -sheet is formed by strands β_3 , β_4 , and the second half of β_2 (Figure 2B). Strands β_1 and β_2 of LckSH3 are connected by the long RT loop that exhibits an irregular antiparallel structure highly similar to that also observed in other SH3 domains (54). The lack of stable elements of regular secondary structure is confirmed by the absence of slowly exchanging amide protons in D_2O and by the decreased heteronuclear NOE for residues S18–G21 located in the central turn of the RT loop (Figure 3A). The β -strands and the RT loop enclose a hydrophobic core that is formed by the nonpolar amino acids V9, A11, L23, F25, L31, I33, A43, I54, P55, and V59 which are buried in the interior of the protein (Figure 3B). Strands β_2 and β_3 , and β_3 and β_4 , are connected by the n-src and distal loop, respectively. The decreased heteronuclear NOE observed for residues S37 and G38 (Figure 3A) suggests an increased flexibility, and therefore no restraints derived from dipolar couplings were included for the corresponding residues in order to avoid errors due to conformational averaging. Numerous long-range NOEs originating from residues L34, E35, E39, and W40, however, indicate that dynamics is only a local phenomenon mainly restricted to residues S37 and G38. The conformation of the turn connecting strands β_4 and β_5 slightly deviates from a regular 3_{10} -helical conformation that is frequently observed in other SH3 domains (53, 54). In our set of structures residues 56–58 adopt helix-typical φ/ψ angle combinations, but a backbone hydrogen bond between residues 56 and 59 expected for this structural element clearly proved to be inconsistent with the residual dipolar couplings.

In summary, the structure of LckSH3 determined in the present study is highly similar to the crystal structure of the LckSH3 domain in the SH2–SH3 domain pair (55) as evidenced by a backbone RMSD of 0.96 Å for residues 7–61 between both structures (Figure 2A). The differences are mainly located in the loops connecting the strands of the β -sheet and can at least partially be explained by crystal packing: Residues H13, Y15, E16, E39, W40, P55, N57, and F58 are part of the dimer interface that is formed with the SH2 domain of the second domain pair in the asymmetric unit of the crystal (55). In addition, the RT and n-src loops exhibit the most prominent dynamics in the molecule, and differences between the conformation in solution and in the crystal have also been reported in a previous NMR study (56).

As known from the structures of SH3–ligand complexes binding of proline-rich peptides occurs at a shallow hydrophobic patch formed by residues of the RT loop, the n-src loop, and the helical turn connecting strands β_4 and β_5 (54, 57). In this region several solvent-exposed aromatic amino acids (H13, Y15, W40, F53, F58) are found in LckSH3 (Figure 2B) representing together with the highly conserved P55 and N57 potential candidates for Tip interaction.

Structural Features of Tip Important for Interaction with SH3 Domains. CD spectroscopy was used to assess the structural properties of Tip(173–185) and Tip(168–187) in solution prior to SH3 binding. Both peptides contain the polyproline motif ($^{176}\text{TPPLPPR}^{183}$) but differ in the number of flanking residues. Additional CD spectra were measured for the W170L mutant of Tip(168–187) that was used for the fluorescence titration experiments.

The CD spectra of all three peptides investigated are very similar and are dominated by a negative band with a minimum at 203 nm (Figure 4) indicative of the existence of a type II polyproline (PPII) helix (24, 58) that has an intense minimum at 204 nm. The observation that the spectra of 13-mer and 20-mer Tip fragments are virtually identical is most likely due to the fact that the PPII helix is the structural element giving the major contribution to the CD signal at 204 nm ($\Theta_{\text{MRW}} \sim 40000 \text{ deg cm}^2 \text{ dmol}^{-1}$) and that this helix exhibits a very similar length in all of the peptides while the flanking regions give no dominant contribution to the CD signal around 203 nm.

The ellipticity of 16 mdeg ($\Theta_{\text{MRW}} \sim 25000 \text{ deg cm}^2 \text{ dmol}^{-1}$) measured for Tip(173–185) at 204 nm corresponds to approximately two-thirds of the value observed for an ideal PPII helix (58). Similar portions of PPII content were also observed for other unbound natural proline-rich sequences known to interact with SH3 domains (24). Preexistence of a PPII helix, however, appears not to be a prerequisite for SH3 binding, as evidenced by a proline-rich peptide derived from the p85 subunit of PI 3-kinase that is unstructured in the unbound state (59).

A more detailed inspection of the Tip CD spectra reveals that the weak positive maximum at 228 nm which is typical for ideal PPII helices ($\Theta_{\text{MRW}} \sim 3000 \text{ deg cm}^2 \text{ dmol}^{-1}$) is not present in the Tip peptides investigated here. In principle, the absence of the 228 nm band could be due to the presence of aromatic amino acids (60). In the Tip peptides investigated, however, the only aromatic amino acid is W170 in Tip(168–187), and an effect of this residue clearly can be ruled out because the W170L mutant shows a virtually

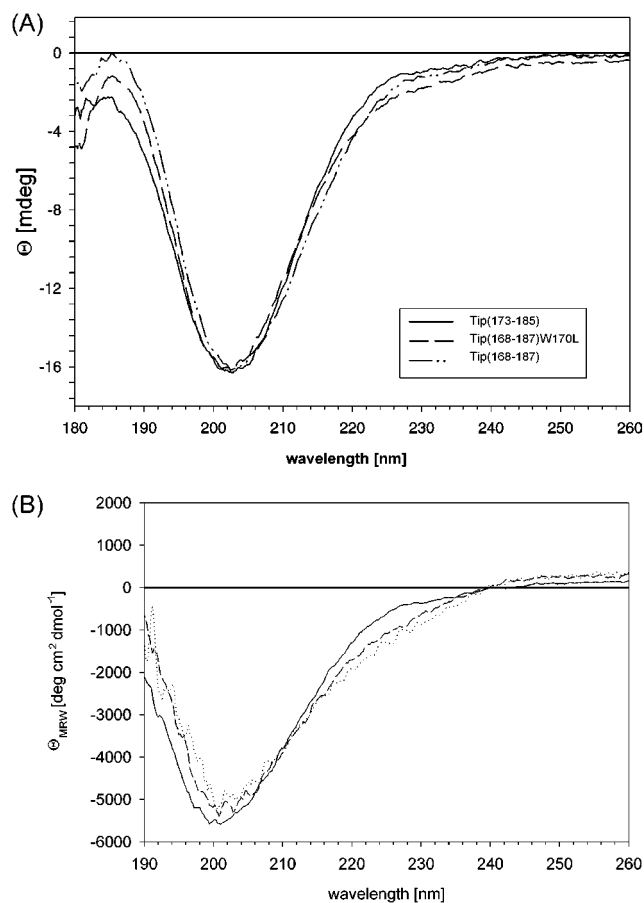


FIGURE 4: (A) Far-UV CD spectra of three different Tip peptides containing the proline-rich motif. Spectra were collected at pH 6.3 and 50 μM sample concentration. (B) Far-UV CD spectra of Tip(168–187) upon addition of 30% and 50% TFE collected at pH 6.3 with a starting concentration of 5 μM Tip(168–187). CD spectra measured at 0%, 30%, and 50% TFE concentration are shown as solid, dashed, and dotted lines, respectively.

identical CD spectrum (Figure 4A). The absence of this positive band was also observed for other proline-rich peptides (24) and has been interpreted by the presence of β -turn conformations that give rise to a negative band at 225 nm (58).

To further investigate the intrinsic conformational stability of the Tip peptides, a TFE titration experiment was performed for Tip(168–187). In principle, this type of study shall prove whether the peptides are able to adopt some alternative conformations in which intramolecular hydrogen bonds are formed (24). TFE was reported to favor intramolecular hydrogen bond formation at the expense of solvent hydrogen bonding (61) and can therefore be used as a probe to explore the existence of alternative elements of secondary structure (24).

Titration of Tip(168–187) with TFE (Figure 4B) indicated that the conformational changes are small even in the presence of 50% TFE. In summary, CD spectroscopy (Figure 4A) proves that the PPII helix is already predefined in the unbound Tip peptides and there is no evidence from TFE titration experiments (Figure 4B) for the formation of alternative elements of secondary structure in Tip(168–187).

Generally, SH3 ligands are pseudosymmetrical and may therefore bind in one of two opposite orientations (62, 63), and it was shown that peptides that bind in one or the other

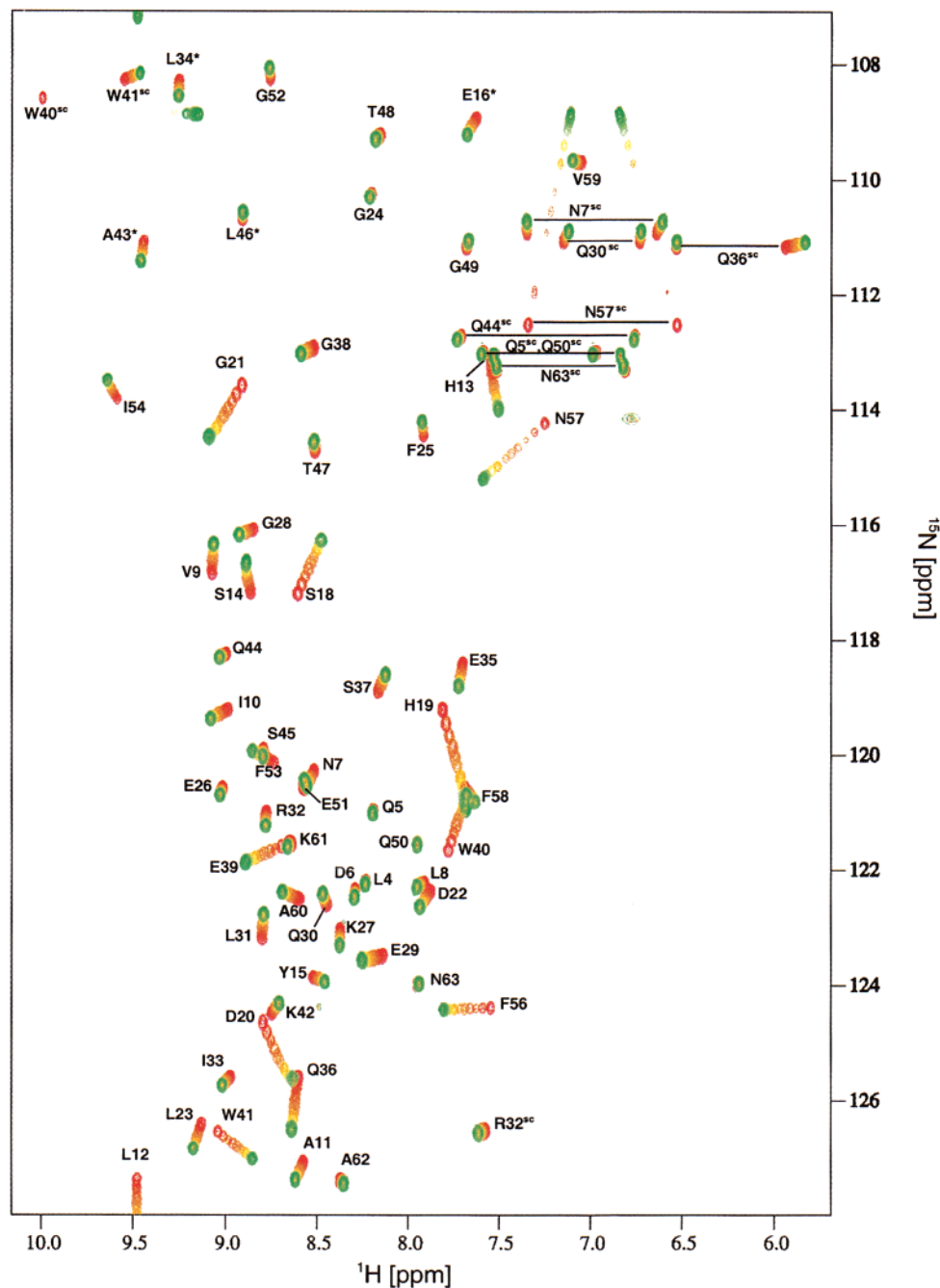


FIGURE 5: NMR titration experiment showing the changes in the ^{15}N , ^1H HSQC spectrum of free LckSH3 (red) upon gradual addition of Tip(173–185). Resonances belonging to the spectra after the final step of the titration (4-fold molar excess of Tip) are shown in green. Resonances are labeled with the corresponding sequence positions. Side-chain (sc) NH_2 resonances for glutamines and asparagines are connected. Aliased resonances are marked with an asterisk.

orientation share different consensus motifs. Specifically, ligands that bind in the class I or class II orientation conform the consensus $+\text{p}\Psi\text{Pp}\Psi\text{P}$ or $\Psi\text{Pp}\Psi\text{Pp}+$, respectively, where the upper case positions represent conserved residues that contact the SH3 domain and confer specificity and the lower case residue positions represent scaffolding residues that tend to be proline (64). Ψ and $+$ indicate sequence positions occupied by aliphatic and basic residues, respectively. The sequence of the proline-rich motif of Tip ($^{176}\text{TPPLPPRP}^{183}$) allows Tip to be classified as a type II ligand because it exhibits an identical sequence for six out of seven positions of the class II consensus motif. The only deviation is the presence of Thr176 instead of a hydrophobic residue that is preferentially observed at this position. A threonine or

arginine is also observed at the corresponding sequence position in the proline-rich motif of the HIV-1 Nef protein, which also binds in a class II orientation (65–67). The importance of this sequence position was shown by the fact that a $\text{T} \rightarrow \text{R}$ mutation in HIV-1 Nef significantly increases the binding affinity (68).

Investigation of the Tip–LckSH3 Interaction by NMR Spectroscopy. Information about those residues of LckSH3 involved in Tip binding was obtained from NMR titration experiments. The process of the NMR titration experiments resulting from gradual addition of Tip(173–185) to ^{15}N -labeled LckSH3 is shown in Figure 5. The most prominent changes of the chemical shifts were observed for three stretches of the peptide chain (S18–G21, Q36–W41, F53–

N57) corresponding to the RT loop, the n-src loop, and a helical turn connecting strands β_4 and β_5 (Figures 1, 2, and 6). These regions are generally known to form the major part of the binding surface for proline-rich peptides (54). In addition, distinct changes of the chemical shifts were also observed for residues I10–L12 and F58–A60 corresponding to strands β_1 and β_5 of the β -sheet.

The structure of the LckSH3 was investigated in the presence of a 4-fold molar excess of Tip(168–187). Analysis of the NOE pattern including more than 150 unambiguously assigned NOEs revealed that the Tip-bound structure is virtually identical to the free SH3 (data not shown), indicating that the changes of the chemical shifts are due to very subtle structural rearrangements or result from direct interaction with the Tip peptide. Measuring residual dipolar couplings for the Tip–LckSH3 complex that would allow a more detailed characterization of minor structural changes was not possible, because no stable liquid crystal phases were obtained.

The fact that complex formation is in fast chemical exchange on the NMR time scale as evidenced by the continuous change of the chemical shifts upon Tip titration (Figure 5) rendered it impossible to obtain distance information from intermolecular NOE data, which is necessary for the calculation of a high-resolution complex structure. Additional problems arose from the fact that some of the resonances got broadened at a 1–3-fold molar excess of Tip(168–187), indicating the presence of more complex exchange phenomena on the NMR time scale.

Changes in the dynamics of LckSH3 upon complex formation were monitored by comparing the heteronuclear NOE and exchange rates in D_2O between the free and the Tip-bound form. A significant increase (>20%) of the heteronuclear NOE was observed for residues S18 and S37 located in the RT loop and n-src loop, respectively, that are both in close proximity to the Tip binding site. Addition of Tip also resulted in markedly longer exchange lifetimes of the LckSH3 backbone amides: For a total of 12 residues mainly located in the β -strands exchange rates are decreased by a factor >3. Similar results were reported previously for ligand binding of HckSH3 (69, 70) and for SrcSH3 (63, 71).

Model of the Tip–LckSH3 Complex. A model of the Tip–LckSH3 complex was generated using SrcSH3 in complex with the high-affinity ligand APP12 (63) as a template. APP12 exhibits the identical sequence as Tip for the six residues (PPLPPR) forming the core of the proline helix. The backbone atoms of ligand-bound SrcSH3 and of unbound LckSH3 are superimposable with 1.1 Å RMSD, confirming that SH3 domains generally have similar structures which undergo only minor structural changes upon ligand binding (54). The Tip–LckSH3 complex was modeled by docking Tip to the SH3 domain assuming an identical orientation as in the SrcSH3–APP12 complex followed by 100 steps of conjugate gradient energy minimization. In that way, modeling of residues 176–183 of Tip was possible while a reliable modeling of the additional residues was impeded by the lack of sequence homology to APP12.

The location of Tip residues 176–183 in the complex is in good agreement with the NMR chemical shift data from the titration experiments: All residues showing changes of their normalized shifts larger than 0.12 ppm are in direct

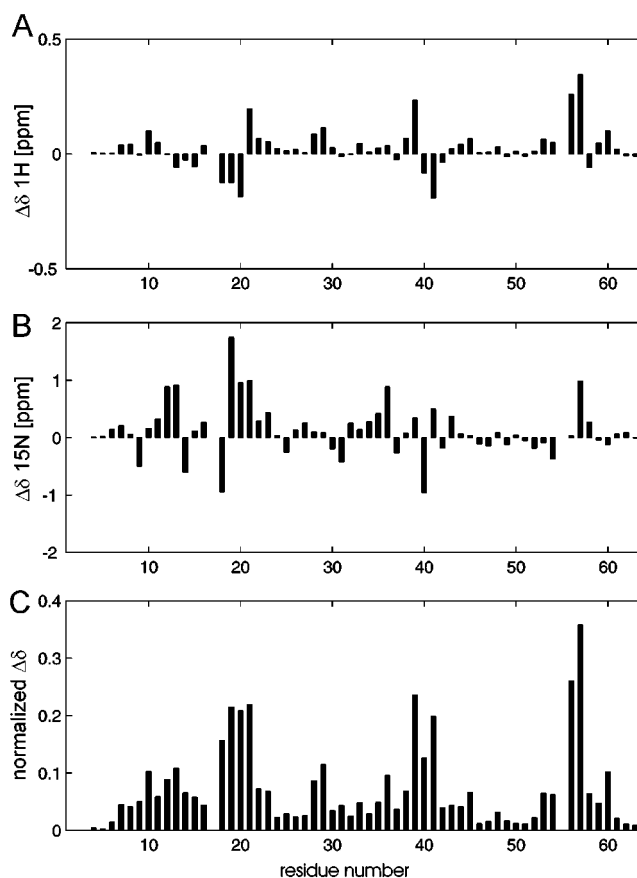


FIGURE 6: Histogram of the change in amide proton (A) and nitrogen (B) resonance chemical shifts of LckSH3 after titration with a 4-fold molar excess of Tip(173–185). The normalized values of the chemical shifts given in (C) were calculated as $\Delta_{\text{norm}} = [(\Delta_{\text{HN}})^2 + (\Delta_{\text{N}}/10)^2]^{1/2}$.

contact with the proline-rich motif of Tip (Figure 7). Looking at the residues exhibiting moderate changes of their normalized chemical shifts >0.04 ppm (Figure 6C), the model reveals that, in particular, those that are located in strands β_1 and β_5 of LckSH3 are not covered by the proline-rich motif. These shifts might be attributed either to direct contacts arising from the residues flanking the proline-rich motif which are not present in the model or to an indirect transmission of those structural rearrangements occurring in the RT loop, the n-Src loop, or the helical turn preceding strand β_5 .

For the Src SH3 domain it was reported that ligand binding can induce strain in the intramolecular hydrogen-bonding network even involving strands β_1 and β_5 of the SH3 domain which are remote from the bound ligand (72). This transmission of structural rearrangements after ligand binding to remote regions of the molecule was suggested to play a role in changing the SH3–SH2 interface formed by strands β_1 , β_2 , and β_5 of the SH3 domain (72).

Molecular Factors Determining the Tip Binding Affinity. The affinity of Tip(173–185) and Tip(168–187) for different SH3 domains was determined by fluorescence spectroscopy (Table 2). The W170L mutant of Tip(168–187) was used in order to allow an undisturbed detection of the SH3 fluorescence.

For the SH3 domains from Lck, Lyn, Hck, Src, Fyn, and Yes binding affinities between 2 and 70 μM were calculated (Table 2), which is the same range as the values reported

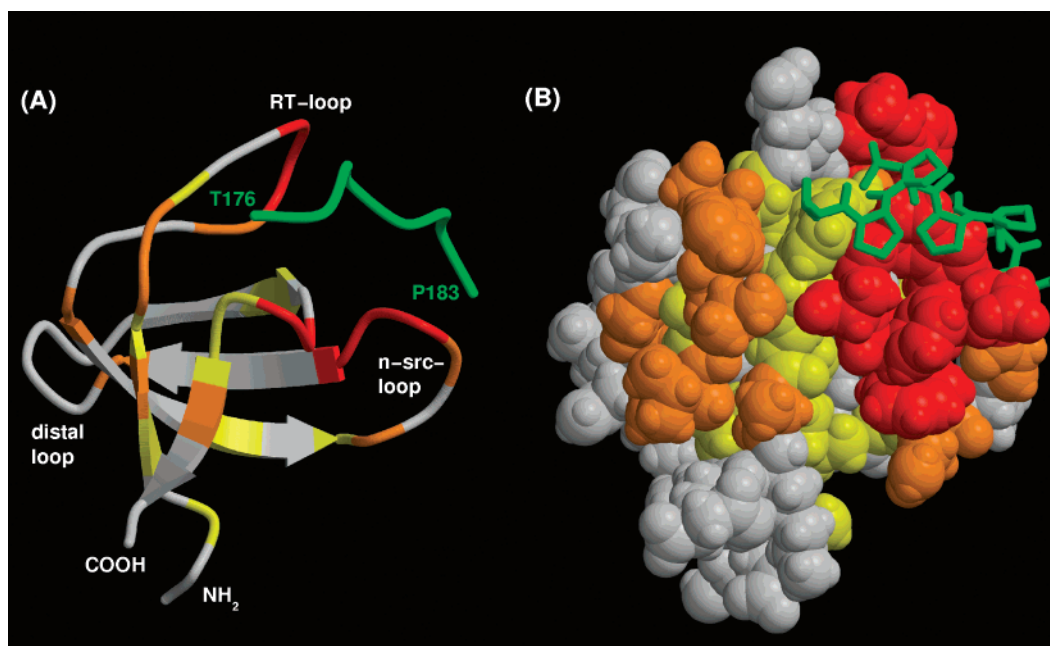


FIGURE 7: (A) Backbone presentation of the Tip(176–183)–LckSH3 complex model generated from the structure of unbound LckSH3 and the SrcSH3–APP12 complex (see text). Residues of LckSH3 are color coded according to the magnitude of the changes of their normalized chemical shifts (Δ_{norm}) upon Tip titration. The color coding is as follows: red, $\Delta_{\text{norm}} > 0.12$ ppm; orange, $0.12 \text{ ppm} \geq \Delta_{\text{norm}} > 0.06$ ppm; yellow, $0.06 \text{ ppm} \geq \Delta_{\text{norm}} > 0.04$ ppm; white, $\Delta_{\text{norm}} \leq 0.04$ ppm. Residues of Tip are shown in green. (B) Space-filled representation of the LckSH3 domain with the bound Tip as a stick representation. Same view and color coding as in (A). Figure prepared with Molscript (51) and Raster3D (52).

Table 2: Affinity Measurements of Proline-Rich Tip Peptides for GST-Tagged SH3 Domains^a

GST–SH3	K_d (μM)	
	Tip(168–187) W170L	Tip(173–185)
Lyn	1.88 ± 0.22	9.58 ± 0.95
Hck	3.15 ± 0.31	12.03 ± 0.37
Lck	8.70 ± 0.77	30.13 ± 1.06
Src	20.51 ± 3.10	44.31 ± 1.26
Fyn	50.58 ± 6.62	63.99 ± 5.46
Yes	53.69 ± 5.17	71.59 ± 3.77
Abl	nt	nb
PLC γ	nb	nt
PI3K p85	nb	nb

^a The values were determined from fluorescence titration experiments. The W170L mutant of Tip(168–187) was used in order to allow an undisturbed detection of the SH3 fluorescence. nt = not tested; nb = not binding.

for the interaction of other proline-rich peptides with SH3 domains (64, 73, 74). No binding of Tip was observed for the SH3 domains from Abl, PLC- γ , and PI3K in the fluorescence titration experiments, indicating that the affinity is lower than 300 μM , and binding may therefore be regarded as nonspecific.

Generally, a stronger binding to Src family SH3 domains was observed for Tip(168–187) compared to Tip(173–185). The overall differences in binding affinity, however, are always less than 1 order of magnitude, which is smaller than those effects reported for several point mutations within or directly adjacent to the proline-rich motif (75). These observations suggest that the additional residues in Tip(168–187) may form additional interactions but do not represent major determinants of binding affinity and specificity.

The classification of Src family tyrosine kinases into groups A and B based on sequence and structural considerations (76) is also reflected in their Tip binding affinity:

Members of group B (Lyn, Hck, Lck) generally bind tighter to Tip than those of group A (Src, Fyn, Yes).

A similar affinity pattern has been observed previously for the HIV-1 Nef protein (77) and peptides derived from Herpesvirus atelans Tio protein (78). As in Tip, the four key residues (in capital letters) of the class II consensus binding motif $\Psi\text{Pp}\Psi\text{Pp}+$ are conserved in these two proteins (Tip, ¹⁷⁶tPpLPpR¹⁸²; Tio, ¹⁸⁸pPqLPpR¹⁹⁴; Nef, ⁷¹tPqVPIR⁷⁷).

Comparison of those SH3 residues that constitute the ligand binding interface (Figure 1) reveals several sequence positions that may account for the differences in binding affinity. In the RT loop the largest differences between group A and group B kinases are observed at sequence positions 18 and 19 while the most significant differences within the group B kinases are found at position 17. In addition, group A and B kinases differ in the presence of a one-residue insertion in the n-src loop (Figure 1).

Generally, a more profound understanding of the role of single residues for modulating binding affinity will require data on both the structure and the dynamics of the systems investigated as suggested by several recent NMR relaxation studies that have pointed out that the affinity of ligand binding can frequently not fully be explained by static pictures (71, 81, 82).

While there are numerous SH3 structures already available, a more detailed comparison of the dynamics based on the ¹⁵N relaxation studies for the unbound HckSH3 (83) and SrcSH3 (71) which differ significantly in the Tip binding affinity is hampered by the fact that the ¹H–¹⁵N cross-peaks of residues 18–20 in the RT loop were not detectable in the NMR spectra of HckSH3 (83), impeding a further characterization.

This present study shows that Tip can interact with the SH3 domains of several Src family tyrosine kinases. Further

structural investigations will have to prove whether the molecular details of the corresponding Tip–SH3 interactions are the same as observed for the Tip–LckSH3 complex. In particular, it will be interesting to see whether Tip binding generally affects the residues of the β -strands close to the SH3–SH2 interface as detected by the chemical shift changes in our NMR experiments for the Tip–LckSH3 interaction (Figure 7). This feature is of particular interest in light of the fact that the SH3–SH2 domain orientation plays a critical role for kinase regulation in general, and the exceptional structural properties of this interface in Lck have recently been pointed out by Arold et al. (80). Thus, secondary effects of Tip binding mediated via the SH3–SH2 domain interface might confer additional specificity to the Tip–SH3 interaction.

ACKNOWLEDGMENT

We thank Ulrike Herzing for excellent technical assistance.

REFERENCES

- Sefton, B. M. (1991) *Oncogene* 6, 683–686.
- Straus, D. B., and Weiss, A. (1992) *Cell* 70, 585–593.
- Anderson, S. J., Levin, S. D., and Perlmutter, R. M. (1994) *Adv. Immunol.* 56, 151–178.
- Xu, W., Harrison, S. C., and Eck, M. J. (1997) *Nature* 385, 595–602.
- Williams, J. C., Weijland, A., Gonfloni, S., Thompson, A., Courtneidge, S. A., Superti-Furga, G., and Wierenga, R. K. (1997) *J. Mol. Biol.* 274, 757–775.
- Sicheri, F., Moarefi, I., and Kuriyan, J. (1997) *Nature* 385, 602–609.
- Mustelin, T., and Altman, A. (1990) *Oncogene* 5, 809–813.
- Moarefi, I., LaFevre-Bernt, M., Sicheri, F., Huse, M., Lee, C. H., Kuriyan, J., and Miller, W. T. (1997) *Nature* 385, 650–653.
- Watts, J. D., Affolter, M., Krebs, D. L., Wange, R. L., Samelson, L. E., and Aebersold, R. (1994) *J. Biol. Chem.* 269, 29520–29529.
- Jung, J. U., Choi, J. K., Ensser, A., and Biesinger, B. (1999) *Semin. Cancer Biol.* 9, 231–239.
- Biesinger, B., Müller-Fleckenstein, I., Simmer, B., Lang, G., Wittmann, S., Platzer, E., Desrosiers, R. C., and Fleckenstein, B. (1992) *Proc. Natl. Acad. Sci. U.S.A.* 89, 3116–3119.
- Dubois, S. M., Guo, J., Czajak, S., Desrosiers, R. C., and Jung, J. U. (1998) *J. Virol.* 72, 1308–1313.
- Biesinger, B., Tsygankov, A. Y., Fickenscher, H., Emmrich, F., Fleckenstein, B., Bolen, J. B., and Bröker, B. M. (1995) *J. Biol. Chem.* 270, 4729–4734.
- Wehner, L. E., Schröder, N., Kamino, K., Friedrich, U., Biesinger, B., and Rütter, U. (2001) *DNA Cell Biol.* 20, 81–88.
- Jung, J. U., Lang, S. M., Friedrich, U., Jun, T., Roberts, T. M., Desrosiers, R. C., and Biesinger, B. (1995) *J. Biol. Chem.* 270, 20660–20667.
- Hartley, D. A., Amdjadi, K., Hurley, T. R., Lund, T. C., Medveczky, P. G., and Sefton, B. M. (2000) *Virology* 276, 339–348.
- Friedrich, U. (1999) Src-Kinase Interaktionen des Herpesvirus samirii Onkoproteins Tip, Dissertation, Friedrich-Alexander-Universität, Erlangen-Nürnberg.
- Jung, J. U., Lang, S. M., Jun, T., Roberts, T. M., Veillette, A., and Desrosiers, R. C. (1995) *J. Virol.* 69, 7814–7822.
- Wiese, N., Tsygankov, A. Y., Klauenberg, U., Bolen, J. B., Fleischer, B., and Bröker, B. M. (1996) *J. Biol. Chem.* 271, 847–852.
- Lund, T. C., Garcia, R., Medveczky, M. M., Jove, R., and Medveczky, P. G. (1997) *J. Virol.* 71, 6677–6682.
- Lund, T. C., Prator, P. C., Medveczky, M. M., and Medveczky, P. G. (1999) *J. Virol.* 73, 1689–1694.
- Hartley, D. A., Hurley, T. R., Hardwick, J. S., Lund, T. C., Medveczky, P. G., and Sefton, B. M. (1999) *J. Biol. Chem.* 274, 20056–20059.
- Isakov, N., and Biesinger, B. (2000) *Eur. J. Biochem.* 267, 3413–3421.
- Viguera, A. R., Arrondo, J. L., Musacchio, A., Saraste, M., and Serrano, L. (1994) *Biochemistry* 33, 10925–10933.
- Posern, G., Zheng, J., Knudsen, B. S., Kardinal, C., Müller, K. B., Voss, J., Shishido, T., Cowburn, D., Cheng, G., Wang, B., Kruh, G. D., Burrell, S. K., Jacobson, C. A., Lenz, D. M., Zamborelli, T. J., Adermann, K., Hanafusa, H., and Feller, S. M. (1998) *Oncogene* 16, 1903–1912.
- Mori, S., Abeygunawardana, C., O'Neill Johnson, M., and van Zyl, P. C. M. (1995) *J. Magn. Reson.* 108, 94–98.
- Grzesiek, S., and Bax, A. (1992) *J. Magn. Reson.* 96, 432–440.
- Wittekind, M., and Mueller, L. (1993) *J. Magn. Reson.* 101B, 201–205.
- Grzesiek, S., and Bax, A. (1992) *J. Am. Chem. Soc.* 114, 6291–6293.
- Vuister, G. W., and Bax, A. (1993) *J. Am. Chem. Soc.* 115, 7772–7777.
- Zhang, W., Smithgall, T., and Gmeiner, W. H. (1997) *J. Biomol. NMR* 10, 263–272.
- Grzesiek, S., and Bax, A. (1993) *J. Magn. Reson.* 101B, 114–119.
- Grzesiek, S., Anglister, J., and Bax, A. (1993) *J. Magn. Reson.* 101B, 114–119.
- Vuister, G. W., and Bax, A. (1992) *J. Magn. Reson.* 98, 428–435.
- Gehring, K., and Ekiel, I. (1998) *J. Magn. Reson.* 135, 85–193.
- Sattler, M., Schleucher, J., and Griesinger, C. (1999) *Prog. NMR Spectrosc.* 34, 93–158.
- Dayie, K. T., and Wagner, G. (1994) *J. Magn. Reson.* 111A, 121–126.
- Ottiger, M., and Bax, A. (1998) *J. Biomol. NMR* 12, 361–372.
- Ottiger, M., Delaglio, F., and Bax, A. (1998) *J. Magn. Reson.* 131, 373–378.
- Johnson, B. A., and Blevins, R. A. (1994) *J. Biomol. NMR* 4, 603–614.
- Brünger, A. T. (1993) *X-PLOR Version 3.1*, Howard Hughes Medical Institute and Yale University, New Haven, CT.
- Nilges, M., and O'Donoghue, S. I. (1998) *Prog. NMR Spectrosc.* 32, 107–139.
- Folmer, R. H., Hilbers, C. W., Konings, R. N., and Nilges, M. (1997) *J. Biomol. NMR* 9, 245–258.
- Kuszewski, J., and Clore, G. M. (2000) *J. Magn. Reson.* 146, 249–254.
- Neudecker, P., Sticht, H., and Rösch, P. (2001) *J. Biomol. NMR* 21, 373–375.
- Losonczy, J. A., Andreac, M., Fischer, M. W., and Prestegard, J. H. (1999) *J. Magn. Reson.* 138, 334–342.
- Kabsch W., and Sander, C. (1983) *Biopolymers* 22, 2577–2637.
- Koradi, R., Billeter, M., and Wüthrich, K. (1996) *J. Mol. Graphics* 14, 51–55.
- Laskowski, R. A., MacArthur, M. W., Moss, D. S., and Thornton, J. M. (1993) *J. Appl. Crystallogr.* 26, 283–291.
- Hutchinson, E. G., and Thornton, J. M. (1996) *Protein Sci.* 5, 212–220.
- Kraulis, P. (1991) *J. Appl. Crystallogr.* 24, 946–950.
- Merritt, E. A., and Murphy, M. E. P. (1994) *Acta Crystallogr. D50*, 869–873.
- Morton, C. J., Pugh, D. J. R., Brown, E. L. J., Kahmann, J. D., Renzoni, D. A. C., and Campbell, I. D. (1996) *Structure* 4, 705–714.
- Larson, S. M., and Davidson, A. R. (2000) *Protein Sci.* 9, 2170–2180.
- Eck, M. J., Atwell, S. K., Shoelson, S. E., and Harrison, S. C. (1994) *Nature* 368, 764–769.
- Hiroaki, H., Klaus, W., and Senn, H. (1996) *J. Biomol. NMR* 8, 105–122.

57. Morton, C. J., and Campbell, I. D. (1994) *Curr. Biol.* 4, 615–617.
58. Fasman, G. D. (1996) *Circular Dichroism and the Conformational Analysis of Biomolecules*. Plenum Press, New York.
59. Renzoni, D. A., Pugh, D. J., Siligardi, G., Das, P., Morton, C. J., Rossi, C., Waterfield, M. D., Campbell, I. D., and Ladbury, J. E. (1996) *Biochemistry* 35, 15646–15653.
60. Vuilleumier, S., Sancho, J., Loewenthal, R., and Fersht, A. R. (1993) *Biochemistry* 32, 10303–10313.
61. Sönnichsen, F. D., Van Eyk, J. E., Hodges, R. S., and Sykes, B. D. (1992) *Biochemistry* 31, 8790–8798.
62. Kuriyan, J., and Cowburn, D. (1997) *Annu. Rev. Biophys. Biomol. Struct.* 26, 259–288.
63. Feng, S., Kasahara, C., Rickles, R. J., and Schreiber, S. L. (1995) *Proc. Natl. Acad. Sci. U.S.A.* 92, 12408–12415.
64. Sparks, A. B., Rider, J. E., Hoffman, N. G., Fowlkes, D. M., Quillam, L. A., and Kay, B. K. (1996) *Proc. Natl. Acad. Sci. U.S.A.* 93, 1540–1544.
65. Grzesiek, S., Bax, A., Clore, G. M., Gronenborn, A. M., Hu, J. S., Kaufman, J., Palmer, I., Stahl, S. J., and Wingfield, P. T. (1996) *Nat. Struct. Biol.* 3, 340–345.
66. Lee, C. H., Saksela, K., Mirza, U. A., Chait, B. T., and Kuriyan, J. (1996) *Cell* 85, 931–942.
67. Arold, S., Franken, P., Strub, M. P., Hoh, F., Benichou, S., Benarous, R., and Dumas, C. (1997) *Structure* 5, 1361–1372.
68. Saksela, K., Cheng, G., and Baltimore, D. (1995) *EMBO J.* 14, 484–491.
69. Engen, J. R., Smithgall, T. E., Gmeiner, W. H., and Smith, D. L. (1997) *Biochemistry* 36, 14384–14391.
70. Horita, D. A., Baldissari, D. M., Zhang, W., Altieri, A. S., Smithgall, T. E., Gmeiner, W. H., and Byrd, R. A. (1998) *J. Mol. Biol.* 278, 253–265.
71. Wang, C., Pawley, N. H., and Nicholson, L. K. (2001) *J. Mol. Biol.* 313, 873–884.
72. Cordier, F., Wang, C., Grzesiek, S., and Nicholson, L. K. (2000) *J. Mol. Biol.* 304, 497–505.
73. Alexandropoulos, K., Cheng, G., and Baltimore, D. (1995) *Proc. Natl. Acad. Sci. U.S.A.* 92, 3110–3114.
74. Rickles, R. J., Botfield, M. C., Zhou, X. M., Henry, P. A., Brugge, J. S., and Zoller, M. J. (1995) *Proc. Natl. Acad. Sci. U.S.A.* 92, 10909–10913.
75. Pisabarro, M. T., and Serrano, L. (1996) *Biochemistry* 35, 10634–10640.
76. Williams, J. C., Wierenga, R. K., and Saraste, M. (1998) *Trends Biochem. Sci.* 23, 179–184.
77. Arold, S., O'Brien, R., Franken, P., Strub, M. P., Hoh, F., Dumas, C., and Ladbury, J. E. (1998) *Biochemistry* 37, 14683–14691.
78. Albrecht, J. C., Friedrich, U., Kardinal, C., Koehn, J., Fleckenstein, B., Feller, S. M., and Biesinger, B. (1999) *J. Virol.* 73, 4631–4639.
79. Yan, B. X., and Sun, Y. Q. (1997) *J. Biol. Chem.* 272, 3190–3194.
80. Arold, S. T., Ulmer, T. S., Mulhern, T. D., Werner, J. M., Ladbury, J. E., Campbell, I. D., and Noble, M. E. (2001) *J. Biol. Chem.* 276, 17199–17205.
81. Kay, L. E., Muhandiram, D. R., Wolf, G., Shoelson, S. E., and Forman-Kay, J. D. (1998) *Nat. Struct. Biol.* 5, 156–163.
82. Lee, A. L., Kinnear, S. A., and Wand, A. J. (2000) *Nat. Struct. Biol.* 7, 72–77.
83. Horita, D. A., Zhang, W., Smithgall, T. E., Gmeiner, W. H., and Byrd, R. A. (2000) *Protein Sci.* 9, 95–103.

BI015986J